universe

IMPACT FACTOR 2.5

CITESCORE 4.3

Article

4D Embedded Rotating Black Hole as a Particle Accelerator in the Presence of Magnetic Fields

Abraão J. S. Capistrano, Carlos Henrique Coimbra-Araújo and Rita de Cássia dos Anjos

Topic Collection

Open Questions in Black Hole Physics

Edited by

Dr. Gonzalo J. Olmo and Dr. Diego Rubiera-Garcia

MDPI

https://doi.org/10.3390/universe10090355

universe

MDPI

Article

4D Embedded Rotating Black Hole as a Particle Accelerator in the Presence of Magnetic Fields

Abraão J. S. Capistrano [1,2,*], Carlos Henrique Coimbra-Araújo [1,2] and Rita de Cássia dos Anjos [1,2,3,4,5]

[1] Departamento de Engenharias e Ciências Exatas, Universidade Federal do Paraná, Palotina 85950-000, PR, Brazil; carlos.coimbra@ufpr.br (C.H.C.-A.); ritacassia@ufpr.br (R.d.C.d.A.)
[2] Applied Physics Graduation Program, Federal University of Latin-American Integration, Foz do Iguassu 85867-670, PR, Brazil
[3] Programa de Pós-Graduação em Física e Astronomia, Universidade Tecnológica Federal do Paraná, Jardim das Américas, Curitiba 82590-300, PR, Brazil
[4] Programa de Pós-Graduação em Física, Departamento de Física, Universidade Estadual de Londrina (UEL), Londrina 86057-970, PR, Brazil
[5] Núcleo de Astrofísica e Cosmologia (Cosmo-Ufes), Departamento de Física, Universidade Federal do Espírito Santo, Vitória 29075-910, ES, Brazil
* Correspondence: capistrano@ufpr.br

Abstract: We analyze a rotating black hole (BH) in a four-dimensional space-time embedded in five-dimensional flat bulk. In Boyer–Lindquist coordinates, we use a generic extension of the Kerr metric by the line element of Gürses–Gürsey metric. We discuss their horizon properties and shadow cast which is tailored by the influence of the extrinsic curvature. By means of the model based on the Nash–Greene theorem, we analyze the Gürses–Gürsey metric embedded in five dimensions acting as a rotating "charged" BH which may be regarded as a source of ultrahigh-energy cosmic rays (UHECRs). We also show that this type of BH presents a different structure of the accretion disk which is modified by the extrinsic curvature leading to an enlargement of the photons ring and an increase in the BH's inner shadow. In the presence of a magnetic field, our initial results suggest that such BHs may be efficient free-test particle accelerators orbiting the inner stable circular orbit (ISCO).

Keywords: black hole; Nash–Greene theorem; gravitational field

Citation: Capistrano, A.J.S.; Coimbra-Araújo, C.H.; dos Anjos, R.d.C. 4D Embedded Rotating Black Hole as a Particle Accelerator in the Presence of Magnetic Fields. *Universe* **2024**, *10*, 355. https://doi.org/10.3390/universe10090355

Academic Editors: Gonzalo J. Olmo and Diego Rubiera-Garcia

Received: 24 June 2024
Revised: 29 August 2024
Accepted: 2 September 2024
Published: 4 September 2024

1. Introduction

A renewal of interest in studying black holes (BHs) came from the direct detection of gravitational waves by Laser Interferometer Gravitational-Wave Observatory (LIGO) detectors from two merging stellar mass BH systems [1] in 2016 that opened a new era of possibilities in astronomy, astrophysics and gravitational theories. One of the routes for the understanding of gravity and its relation with the other fundamental interactions, namely the hierarchy problem, considers that the universe is somewhat embedded and evolves in a higher-dimensional space-time. This is not a new idea. Most of these models have been Kaluza–Klein and/or string inspired, such as the seminal works of Arkani-Hamed, Dvali, and Dimopolous (ADD) [2] with a six-dimensional bulk for large extra dimensions where only the sub millimeter gravity accessed and the other gauge interactions remain confined in the four-dimensional space-time. With the use of the Israel–Lanczos junction condition [3], the popular Randall–Sundrum model [4,5] attracted much attention, specifically model II [5] that proposed an infinite five-dimensional model that shared similarities with a four-dimensional model that appealed to the holographic AdS/CFT conjecture [6]. In model II, the so-called three-brane is embedded in a five-dimensional anti-de Sitter (AdS5) space-time focused on an explanation of the behavior of gravity. Another popular high-dimensional model relies on the Dvali–Gabadadze–Porrati [7] model that considers the 3 + 1 Minkowski space-time embedded in a flat five-dimensional bulk. One common characteristic of these models and variants is that the embedding is not completely

defined. Thus, in such models, the embedding is static, i.e., it is fixed to a boundary and/or specific conditions are needed to obtain its dynamics. The extrinsic curvature does not exert any dynamical influence on the relation of the bulk and the embedded space-time and is commonly replaced by those conditions.

Our present work is essentially based on previous communications [8–10] that proposed a five-dimensional model using dynamical embedding using the Nash embedding theorem [11,12] to investigate possible physical consequences of the perturbations of the geometry in embedded spaces. This present framework is different from the standard braneworld models since the extrinsic curvature exerts a fundamental role leading to a dynamical embedding rather than static embedding. Then, we propose a model-independent formulation, avoiding referring to this model as a braneworld model considering all the differences between the formulations. In fact, standard braneworld models may be described as a particular case of the covariant-independent approach presented in this paper and may be regarded as a family of stable perturbations of a given locally embedded background space-time.

Due to the fact that BHs turned out to be one of the crucial elements to understand the behavior of gravity, the study of exact solutions provides an important test for alternative theories of gravity [13–19]. In previous communications, we explored a four-dimensional spherically symmetric geometry embedded in a five-dimensional bulk. For such geometry, we found that a higher space for embedding with a bulk larger than 5 is a must due to strong restrictions on the embedding itself [20]. In this case, the Newtonian limit could not be correctly obtained. We obtained similar results with a classical thermodynamic analysis for the before-mentioned geometry in which global stability was not a preferred state [21]. Moreover, the analysis of the quasinormal frequencies of the BHs produced using the Wentzel, Kramers, and Brillouin (WKB) approximation [22] also indicated serious constraints on embedding models in five dimensions, and the correct analysis of spherically symmetric geometry in an embedded space should be made at least with a six-dimensional bulk. This was effectively implemented in Ref. [23] in which, besides the extrinsic curvature, we had the influence of the torsion vector $A_{\mu ab}$ as a gauge group of rotations $SO(2)$ in the extra dimensions. As a result, we obtained the correct embedding for a spherically symmetric metric producing a lukewarm BH and the appearance of an emergent cosmological constant Λ.

BHs are true accelerators of cosmic particles, capable of generating cosmic rays with unimaginable energies. To explain this phenomenon, some fundamental processes are evoked and take place in the vicinity of black holes, collisional processes [24,25] or those related to particle decay [26] both arising from a process of harnessing gravitational energyor accelerating processes related to electromagnetic fields from the relationship between BHs and plasma structures, such as accretion disks and jets [27–29]. From a broader perspective, BHs are perfect cosmic laboratories for testing fundamental theories, such as the theory of general relativity, but they also serve to scrutinize astrophysical phenomena that are still poorly understood. In astronomy, for example, understanding the behavior of galactic black holes is the same as understanding the formation properties of the host galaxy [30,31]. The gravitational influence of these BHs affects star formation and galactic dynamics. The interplay between these supermassive BHs and the surrounding gas can influence the formation and evolution of galaxies, regulating the rate of star formation and the distribution of matter. Also noteworthy is the case of stellar mass BHs, born from the collapse of massive stars, which provide insights into the process of stellar formation and evolution. The observation of gamma ray burst data associated with the multimessenger astronomy of gravitational wave emission can be a good way to link the way particles accelerate at the edge of stellar BHs. For instance, in both the stellar and galactic cases, the acceleration of particles near black holes can lead to the appearance of UHECRs, which have energies much higher than any particle that can be produced in terrestrial accelerators [25,32–37].

Investigating the origin of these particles and how they propagate through space is one of the main focuses of astroparticle physics. These cosmic messengers can come

from gamma-ray bursts and other extreme phenomena in the universe, but in particular, they can be accelerated at the edge of BHs. The most standard way to understand this is through the acceleration of particles in accretion disks. In these disks, particles are accelerated to speeds close to that of light, thanks to intense electric fields, modulated by the powerful magnetic fields present in the region. This acceleration is the main mechanism for the production of cosmic rays. Another way comes from the fact that many black holes, especially supermassive ones, launch jets of high-energy particles in opposite directions. These jets are composed of matter accelerated to speeds close to that of light and can extend for millions of light-years. It is worth noting, however, that the energies of UHECRs that exceed the Greisen–Zatsepin–Kuzmin (GZK) limit denote energy sources that are not yet understood [27,32,34,38]. A deep understanding of the spectrum beyond GZK can provide important contributions to the link between the phenomenon described here (the acceleration of particles at the edge of black holes from the collisional BSW effect) and the observation of UHECRs. By describing a collisional mechanism for extracting gravitorotational energy from a black hole, the BSW effect suggests that these objects are not only sinks of matter but can also be sources of energy.

In this paper, we maintain the same five-dimensional bulk with a different metric. We investigate some consequences of a vacuum solution of an embedded four-dimensional model of an axially symmetric gravitational field for a rotating BH to obtain a model for the final fate of the gravitational collapse. In the second section, we make highlights of a mathematical review on embeddings and the general mechanism to obtain the induced field equations in four-dimensional space-time starting from a five-dimensional bulk. The third section focuses on an analysis of the line element of the generic extension of the Kerr metric known as the Gürses–Gürsey metric [39], where we obtain the metric's singularity and horizons. In the fourth section, we discuss the geodesic of test particles and collision effects. In the final section, we present our final remarks and prospects.

2. Highlights on Embeddings and Induced Field Equations

To study the physics of embeddings, we simplify our analyses, starting from a classical approach. Mainly motivated from the hierarchy problem of fundamental interactions, the "not-so-new" physical problems such as dark matter and dark energy problems suggest that something is missing in the LHS of Einstein's equations. To solve these issues, embeddings may provide a viable direction to follow. We adopt dynamical embedding to differ from popular braneworld models, where the perturbations are triggered from the confined sources and the brane is generated by a scalar field coupled to gravity that needs a sophisticated mechanism to localize matter on the brane. Generally speaking, in these models, a common practice is to rely on junction conditions that replace the extrinsic curvature by the energy–momentum tensor of the confined sources. In fact, braneworld models may be described as a particular case of the covariant-independent approach presented in this paper.

The general solution for embedding between geometries is credit to J. Nash [11]. The Nash theorem proposes that a stable embedding with a regular map $\mathcal{X} : V_n \to V_D$ $(n < D)$ occurs by means of a smooth and differentiable process. This makes it possible for any embedded metric geometry to be generated continuously through a sequence of small metric orthogonal perturbations such as

$$g_{\mu\nu} = \bar{g}_{\mu\nu} + \delta y\, \bar{k}_{\mu\nu} + (\delta y)^2\, \bar{g}^{\rho\sigma} \bar{k}_{\mu\rho} \bar{k}_{\nu\sigma} \ldots \quad . \tag{1}$$

where $g_{\mu\nu}$ is the perturbed metric and $\bar{k}_{\mu\nu}$ is the extrinsic curvature. The y parameter is an arbitrary spatial coordinate wherein orthogonal perturbations are driven. The overbar sign indicates a background (non-perturbed) quantity.

By definition, written in the Gaussian frame $\{X^A_\mu, \bar{\eta}^A_a\}$, the extrinsic curvature is given by

$$\bar{k}_{\mu\nu} = -\mathcal{X}^A_{,\mu}\, \eta^B_{,\nu} \mathcal{G}_{AB}\ , \tag{2}$$

which tells us how normal unitary vector η^A in the embedded space deviates from the tangent plane. As a result, the embedded geometry bends. This characteristic sounds interesting to investigate physical problems in cosmology and astrophysics with strong gravitational sources. Then, we investigated the extrinsic curvature per se as an orthogonal complement to the tangent component of the gravitational field, $g_{\mu\nu}$. Concerning notation, capital Latin indices are fixed to 5. Small-case Latin indices refer to the only one extra dimension fixed to 1. All Greek indices refer to the embedded space-time running from 1 to 4.

From Equation (1), one obtains Nash's deformation formula given by

$$k_{\mu\nu} = -\frac{1}{2}\frac{\partial g_{\mu\nu}}{\partial y} \,. \tag{3}$$

This is the core of Nash's embedding theorem published in 1954 applied to non-Euclidean metrics [11] and in 1956 to Riemannian metrics [12] and later extended to pseudo-Riemanian manifolds by Greene [40]. This is a key condition for the perturbations of an embedded space inside the bulk. It also imposes a geometric constraint on the deformations of the embedded space. In this framework, these deformations are not arbitrary and can be generated by perturbations along the direction δy orthogonal to the embedded space V_n by the Lie transport of the Gaussian frame $\{X^A_\mu, \bar{\eta}^A_a\}$ that gives

$$\mathcal{Z}^A_{,\mu} = X^A_{,\mu} + \delta y \, \pounds_{\bar{\eta}} X^A_{,\mu} = X^A_{,\mu} + \delta y \, \bar{\eta}^A_{,\mu} \tag{4}$$

$$\eta^A = \bar{\eta}^A + \delta y \, [\bar{\eta}, \bar{\eta}]^A = \bar{\eta}^A \,, \tag{5}$$

where we define a differentiable and regular map by $\mathcal{X} : V_n \to V_D$. In Equation (5), the independent unit vector field, η^A, is orthogonal to V_n and is not affected by perturbations in that direction. This mechanism avoids possible coordinate gauges that may lead to false perturbations. The perturbed coordinate $\mathcal{Z}^A_{,\mu}$ defines a coordinate chart between the bulk and the embedded space-time. Equations (4) and (5) link the freedom of perturbations of the embedded space-time to the bulk once the extra dimensions do not share the same diffeomorphism invariance of the embedded space. In five dimensions, this process is simplified and just one deformation parameter suffices to locally deform the embedded background in the same way as conducted in Equations (4) and (5).

In the present application, we adopt a five-dimensional bulk, V_5, wherein a smaller space, V_4, is isometrically embedded. Then, one defines chart $\mathcal{X} : V_4 \to V_5$ and the bulk metric $\mathcal{G}_{AB}$ as

$$\mathcal{G}_{AB} = \begin{pmatrix} g_{\mu\nu} & 0 \\ 0 & 1 \end{pmatrix} . \tag{6}$$

Consequently, gravitational action S can be defined with confined matter fields as

$$S = -\frac{1}{2\kappa_5^2}\int \sqrt{|\mathcal{G}|}\left({}^5\mathcal{R} + \mathcal{L}^*_m\right) d^5x \,, \tag{7}$$

where κ_5^2 is a fundamental energy scale on the embedded space, and the curly ${}^5\mathcal{R}$ denotes the five-dimensional Ricci scalar of the bulk. The Lagrangian $\mathcal{L}^*_m$ denotes the bulk source Lagrangian.

One important aspect of the embedding is the Gauss and Codazzi equations given by

$${}^5\mathcal{R}_{ABCD}\mathcal{Z}^A{}_{,\alpha}\mathcal{Z}^B{}_{,\beta}\mathcal{Z}^C{}_{,\gamma}\mathcal{Z}^D{}_{,\delta} = R_{\alpha\beta\gamma\delta} + \left(k_{\alpha\gamma}\, k_{\beta\delta} - k_{\alpha\delta}\, k_{\beta\gamma}\right), \tag{8}$$

$${}^5\mathcal{R}_{ABCD}\mathcal{Z}^A{}_{,\alpha}\mathcal{Z}^B{}_{,\beta}\mathcal{Z}^C{}_{,\gamma}\eta^D = k_{\alpha[\beta;\gamma]} \,, \tag{9}$$

where ${}^5\mathcal{R}_{ABCD}$ denotes the five-dimensional Riemann tensor, and $R_{\alpha\beta\gamma\delta}$ is the four-dimensional Riemann tensor. The semicolon sign in Equation (9) represents the ordinary covariant derivative with respect to the metric $g_{\mu\nu}$ and $k_{\alpha[\beta;\gamma]} \equiv k_{\alpha\beta;\gamma} - k_{\alpha\gamma;\beta}$. These equations reflect

the integrability conditions for the embedding to assure the relation of the bulk with the embedded space. The Nash deformation formula in Equation (3) guarantees the dynamics of the embedded space by solving Equations (8) and (9). The bulk Lagrangian source $\mathcal{L}_m^*$ is somewhat independent of the embedding. Since only gravity should access the bulk by the geometrical constraint of Equation (3), $\mathcal{L}_m^*$ is confined as

$$\begin{aligned} \kappa_5^2 T_{\mu\nu}^* &= -8\pi G T_{\mu\nu} \,, \\ \kappa_5^2 T_{\mu a}^* &= 0 \,, \\ \kappa_5^2 T_{ab}^* &= 0 \,, \end{aligned} \tag{10}$$

from the generic components of $\mathcal{T}_{AB}^*$ of the energy–momentum tensor of the bulk. The components $T_{\mu\nu}^*$, $T_{\mu a}^*$, and T_{ab}^* define the energy–momentum of the tangent (tensor), vector, and scalar components of $\mathcal{T}_{AB}^*$. $T_{\mu\nu}$ and G denote the matter gauge fields and the gravitational Newtonian constant, respectively.

As a common practice, the variation in the Einstein–Hilbert action in Equation (7) with respect to the bulk metric $\mathcal{G}_{AB}$ gives higher-dimensional Einstein equations written as

$${}^5\mathcal{R}_{AB} - \frac{1}{2}\mathcal{G}_{AB} = \alpha^\star \mathcal{T}_{AB} \,, \tag{11}$$

where $\alpha^\star$ is the energy scale parameter and $\mathcal{T}_{AB}^*$ is the energy–momentum tensor for the bulk, and the five-dimensional bulk with constant curvature whose related Riemann tensor is

$${}^5\mathcal{R}_{ABCD} = K_*(\mathcal{G}_{AC}\mathcal{G}_{BD} - \mathcal{G}_{AD}\mathcal{G}_{BC}), \quad A \ldots D = 1 \ldots 5 \,,$$

where $\mathcal{G}_{AB}$ denotes the bulk metric components in arbitrary coordinates and constant curvature K_* is either zero (flat bulk) or it can have positive (deSitter) or negative (anti-deSitter) cosmological constant Λ. For a flat bulk, one obtains the four non-perturbed induced gravitational field equations from a five-dimensional bulk as [8–10,41,42]

$$G_{\mu\nu} - Q_{\mu\nu} = 8\pi G T_{\mu\nu} \,, \tag{12}$$

$$k_{\mu[\nu;\rho]} = 0 \,, \tag{13}$$

where $G_{\mu\nu}$ denotes the four-dimensional Einstein tensor and $Q_{\mu\nu}$ is the deformation tensor. The non-perturbed extrinsic term $Q_{\mu\nu}$ in Equation (12) is given by

$$Q_{\mu\nu} = k_\mu^\rho k_{\rho\nu} - k_{\mu\nu} h - \frac{1}{2}\Big(K^2 - h^2\Big) g_{\mu\nu} \,, \tag{14}$$

where we denote the mean curvature by $h^2 = h \cdot h$ and $h = g^{\mu\nu} k_{\mu\nu}$ and the Gaussian curvature by $K^2 = k^{\mu\nu} k_{\mu\nu}$. By direct derivation, Equation (14) is conserved in the sense that

$$Q_{\mu\nu;\mu} = 0 \,. \tag{15}$$

3. A Gürses–Gürsey Metric Embedded in Five-Dimensions

In the present application, we are interested in realizing how the extrinsic effect unfolds in this gravitational system. Then, we consider a vacuum solution of a four-dimensional axially symmetric gravitational field. In Boyer–Lindquist coordinates, we start with a generic extension of the Kerr metric, i.e., the line element of the Gürses–Gürsey metric [39] written as

$$ds^2 = \left(\frac{2rf(r)}{\rho^2} - 1\right) dt^2 - \frac{4arf(r)\sin^2\theta}{\rho^2} dt d\phi + \frac{\rho^2}{\Delta} dr^2 + \rho^2 d\theta^2 + \frac{\Sigma}{\rho^2}\sin^2\theta d\phi^2 \,, \tag{16}$$

where we have introduced the notation $\rho^2 = a^2\cos^2\theta + r^2$, $\Delta = a^2 + r^2 - 2rf(r)$ and $\Sigma = (r^2 + a^2)^2 - a^2\Delta\sin^2\theta$ at the scale $a = J/m$, in which J is the angular momentum and

m is a rotating mass. The function $f(r)$ is an arbitrary function of the radial coordinate r. In principle, it should absorb a non-trivial effect from extrinsic geometry as a result of the embedding. In other words, we should calculate Equation (13) to realize how the extrinsic effects propagate in the main field equation, i.e., Equation (12). Clearly, when $f(r) = m = constant$, one obtains the standard Kerr solution, and fixing $a = 0$ and $f(r) = m$, we recover the standard Schwarzchild metric. Thus, the solution of Equation (13) can be generically written as

$$k_{\mu\nu} = p_\mu g_{\mu\nu} \quad (no\ sum\ on\ \mu)\ , \tag{17}$$

where $p_\mu = \{p_1(r,\theta,\phi,t), p_2(r,\theta,\phi,t), p_3(r,\theta,\phi,t), p_4(r,\theta,\phi,t)\}$ is a generic coordinate function.

Taking Equations (17) and (13), one obtains (with no sum for μ)

$$Q_{\mu\nu} = p_\mu^2 g_{\mu\nu} - \left(\sum_\alpha p_\alpha\right) p_\mu g_{\mu\nu} - \frac{1}{2}\left(\sum_\alpha p_\alpha^2 - \left(\sum_\alpha p_\alpha\right)^2\right) g_{\mu\nu}\ ,$$

where we can identify

$$U_\mu = p_\mu^2 - \left(\sum_\alpha p_\alpha\right) p_\mu - \frac{1}{2}\left(\sum_\alpha p_\alpha^2 - \left(\sum_\alpha p_\alpha\right)^2\right) \delta_\mu^\mu\ ,$$

and we can write the quantity $Q_{\mu\nu}$ in terms of p_μ as

$$Q_{\mu\nu} = U_\mu g_{\mu\nu} \quad (no\ \ sum\ \ on\ \ \mu)\ . \tag{18}$$

As $Q_{\mu\nu}$ is a conserved quantity, we can find six equations regarding $\sum_\nu g^{\mu\nu} U_{\mu;\nu} = 0$. After carrying out a calculation, one finds only two independent equations

$$\begin{cases} U_1 = p_1^2 - \left(\sum_{\alpha=1}^4 p_\alpha\right) p_1 - \frac{1}{2}\left(\sum_{\alpha=1}^4 p_\alpha^2 - \left(\sum_{\alpha=1}^4 p_\alpha\right)^2\right) \\ U_2 = p_2^2 - \left(\sum_{\alpha=1}^4 p_\alpha\right) p_2 - \frac{1}{2}\left(\sum_{\alpha=1}^4 p_\alpha^2 - \left(\sum_{\alpha=1}^4 p_\alpha\right)^2\right) \end{cases}$$

and the relations

$$\begin{cases} p_1 = p_2 = \alpha(r,\theta)\ , \\ p_3 = p_4 = \beta(r,\theta)\ , \end{cases}$$

where $\alpha(r,\theta) = \alpha$ and $\beta(r,\theta) = \beta$ are generic functions from the direct integration of the functions in $\sum_\nu g^{\mu\nu} U_{\mu;\nu} = 0$. Hence, calculating U_μ quantities, taking into account that $U_1 = U_2$ and $U_3 = U_4$, we write $Q_{\mu\nu}$ as

$$Q_{\mu\nu} = \frac{1}{2}(4\alpha\beta + \alpha^2 + \beta^2) g_{\mu\nu}\ . \tag{19}$$

Assuming the simplest isotropic solution when $\alpha = \beta$, one obtains

$$Q_{\mu\nu} = 3\alpha^2 g_{\mu\nu}\ . \tag{20}$$

In order to determinate the function $f(r)$, we insert Equation (20) into the scalar gravitational equation of Equation (12). In vacuum, with $T_{\mu\nu} = 0$, we rewrite Equation (12) contracted with $g_{\mu\nu}$ in a more convenient form as

$$R_{\mu\nu} + \frac{1}{2} Q = Q_{\mu\nu}\ , \tag{21}$$

where we define the extrinsic scalar as $Q = g^{\mu\nu}Q_{\mu\nu}$. Thus, using Equations (16) and (20), we calculate Equation (21) and obtain the radial equation for the function $f(r)$ as

$$r\frac{d^2f}{dr^2} + \frac{1}{2}\frac{df}{dr} + 6\alpha^2\rho^2 = 0\,. \tag{22}$$

For the choice $\alpha = \frac{\sqrt{\alpha_0}}{\rho}$, we obtain the solution

$$f(r) = c_0 - 4\frac{\alpha_0}{r} + 2\sqrt{r}c_1\,, \tag{23}$$

where the α_0 parameter is regarded as a relic from extrinsic geometry, and c_0 and c_1 are integration constants.

To find the horizons $r = r_H$ of the metric in Equation (16), we start calculating the component $g^{rr} = 0$. Then, we obtain the related inner and outer horizons given by

$$\begin{aligned} r_H^{in} &= 2\,\alpha_1\sqrt{r} + m - \sqrt{4\,\alpha_1^2 r + 4\,\alpha_1 m\sqrt{r} - a^2 + m^2 - 8\,\alpha_0}\,, \\ r_H^{out} &= 2\,\alpha_1\sqrt{r} + m + \sqrt{4\,\alpha_1^2 r + 4\,\alpha_1 m\sqrt{r} - a^2 + m^2 - 8\,\alpha_0}\,. \end{aligned} \tag{24}$$

By the condition $g^{tt} < 0$, we obtain the inner and outer ergospheres as

$$\begin{aligned} r_{ergo}^{in} &= 2\,\alpha_1\sqrt{r} + m - \sqrt{-a^2\cos(\theta)^2 + 4\,\alpha_1^2 r + 4\,\alpha_1 m\sqrt{r} + m^2 - 8\,\alpha_0}\,, \\ r_{ergo}^{out} &= 2\,\alpha_1\sqrt{r} + m + \sqrt{-a^2\cos(\theta)^2 + 4\,\alpha_1^2 r + 4\,\alpha_1 m\sqrt{r} + m^2 - 8\,\alpha_0}\,, \end{aligned} \tag{25}$$

where we appropriately choose $c_0 = m$ and $c_1 = \alpha_1$.

When extrinsic curvature vanishes, setting $\alpha_0 = 0$, in the previous results, then we recover the standard Kerr horizons. A real physical curvature singularity is seen in the Kretschmann scalar $R^{\alpha\beta\mu\nu}R_{\alpha\beta\mu\nu} \to \infty$ at $r \to 0$ but it remains finite at $r = \{r_H^{in}, r_H^{out}\}$. A singular ring is found at $r = 0, \theta = \frac{1}{2}\,\pi$ and this result is independent of the presence of extrinsic curvature. Moreover, an important remark is that the zero mass limit of Equation (23) does not lead to a flat Minkowski space of the metric in Equation (16). In order to study a real solution, the radial coordinate is assumed to have one asymptotic region corresponding to $r \to \infty$, but at this limit, the horizons $r = \{r_H^{in}, r_H^{out}\}$ become singular and so is the metric in Equation (16). Clearly, this can be avoided when imposing the boundary $\alpha_1 = 0$ and Equation (23) that results in the simpler form

$$f(r) = m - 4\frac{\alpha_0}{r}\,. \tag{26}$$

As a result, the inner and outer horizons are now given by

$$\begin{aligned} r_H^{in} &= m - \sqrt{-a^2 + m^2 - 8\,\alpha_0}\,, \\ r_H^{out} &= m + \sqrt{-a^2 + m^2 - 8\,\alpha_0}\,. \end{aligned} \tag{27}$$

Moreover, the inner and outer ergospheres are

$$\begin{aligned} r_{ergo}^{in} &= m - \sqrt{-a^2\cos(\theta)^2 + m^2 - 8\,\alpha_0}, \\ r_{ergo}^{out} &= m + \sqrt{-a^2\cos(\theta)^2 + m^2 - 8\,\alpha_0}\,. \end{aligned} \tag{28}$$

When extrinsic curvature vanishes, setting $\alpha_0 = 0$, in the previous results, then the standard Kerr horizons and ergospheres are recovered again. In this case, α_0 is referred as a tidal "extrinsic charge" in resemblance to Kerr–Newman solutions.

Using the free open-source SageMath [43], we obtain Figures 1 and 2. In Figure 1, we propose an ansatz to constrain the *dimensionless* tidal "extrinsic charge" that should have a cosmological magnitude, as defined in Ref. ([44]), given by

$$\alpha_0 = \sqrt{1 - \Omega_{m(0)}}\, h\,, \tag{29}$$

where $h = 0.674$ is the dimensionless Hubble factor and $\Omega_{m(0)} = 0.315$ denotes the current cosmological parameter for matter density content adopting the baseline mean values of 68% intervals of base-ΛCDM model from Planck TT,TE,EE+lowE+lensing [45]. Thus, one obtains $\alpha_0 = 0.558$ and we use it as a reference value.

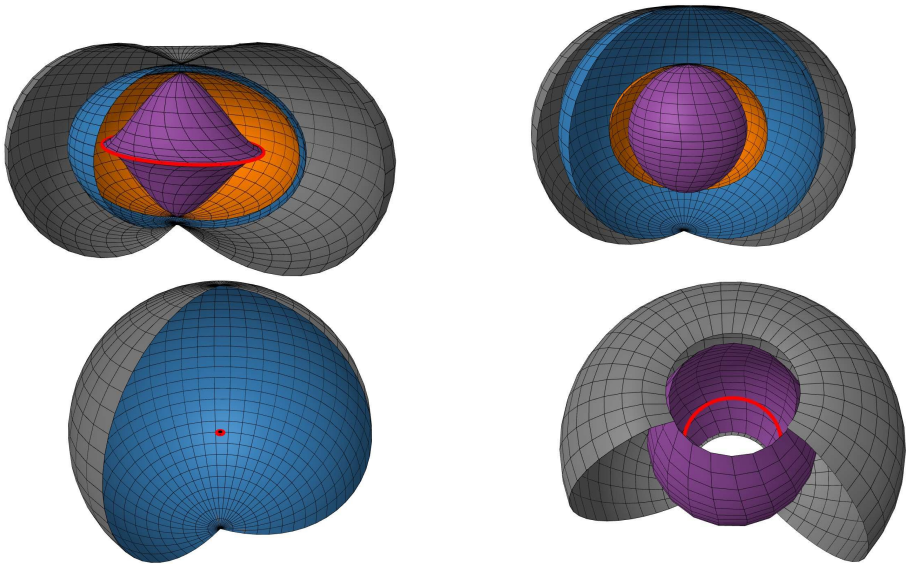

Figure 1. Surfaces in Kerr–Schild coordinates. In the left upper panel, we have the surfaces of the Kerr space-time with $m = 1$ and $a = 0.999$. The upper right panel represents Gürses–Gürsey surfaces for $m = 2.4$ and $a = 0.999$. From left to right regarding the bottom panels, we have Gürses–Gürsey surfaces for $m > 2.4$ and $m < 2.4$ for the same $a = 0.999$. The outer and inner ergosphere, outer and inner horizon and singular ring are colored as grey, lilac, blue, orange, and red, respectively. For an interpretation of the references to color in this figure legend, the reader is referred to the web version of this article.

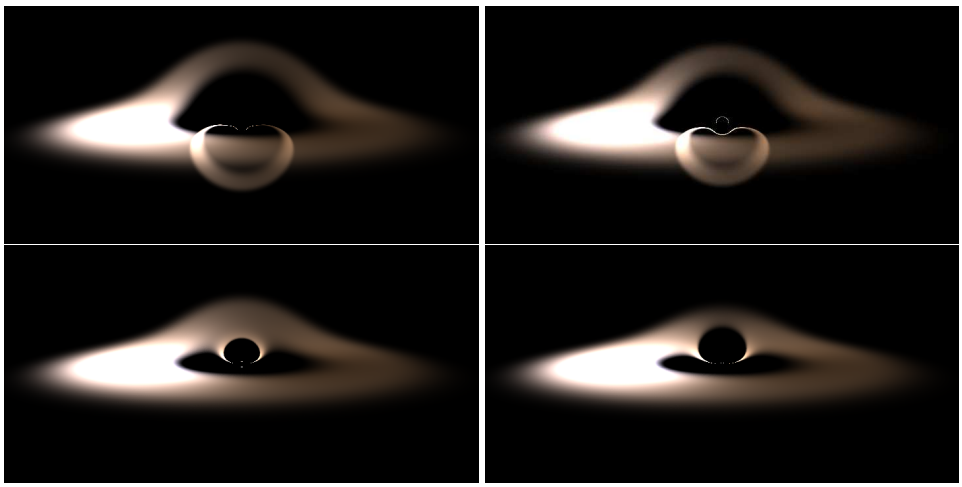

Figure 2. Relativistic aberration to the accretion disk around BHs modified by different values of α_0 for optimal mass $m = 2.4$ and $a = 0.999$.

In Figure 1, we present Gürses–Gürsey surfaces in the upper right and bottom panels. Fixing the values of $\alpha_0 = 0.558$ and $a = 0.999$, for the optimal mass $m = 2.4$, the ring singularity is naked and is shielded by the inner ergosphere. The curvature singularity lies at the kink in the inner ergosurface on the inside. The outer and inner ergosphere and horizons and singular ring are represented as grey, lilac, blue, orange, and red colors, respectively. For masses less than 2.4, the geometry is progressively "mutilated", i.e., all horizons and ergospheres cease to converge to the ring singularity. On the other hand, regarding masses higher than 2.4, the inner horizon and inner ergosphere become progressively smaller up to being shielded by the ring singularity covered by the outer ergosphere and outer horizon. Just for the sake of comparison, Kerr surfaces are represented in the upper left panel. The overall pattern is similar to that described in the case of the Gürses–Gürsey metric. The difference lies in the fact that the masses in Kerr surfaces are lower to maintain the Kerr geometry. Thus, the reference values of mass is fixed at $m = 1$ but masses less than or higher than 1 progressively generate smaller inner horizons and ergospheres up to the ring singularity.

In Figure 2, we compare images with relativistic aberration added to the accretion disk around BHs changed by extrinsic curvature relaxing to different values of α_0.The optimal mass value is $m = 2.4$ for all cases. Scale a is fixed as $a = 0.999$, and from left to right in the upper and bottom panels, we have the results for $\alpha_0 = \{0.4, 0.558, 1.2, 1.5\}$, respectively. We found that higher values of the extrinsic term lead to the enlargement of the photon rings but also with an increase in the BH's inner shadow. It is important to point out that the increase in the shadow comes from an increase in the inner horizons until the image of the disk's underside vanishes. The upper left panel shows a lower value of α_0 and the photon ring is not visible.

4. Geodesic of Test Particles and Collisional Effects

Once the properties of these BHs have been obtained with this approach, we analyze the geodesics of colliding classical charged particles at the BH stable orbits. For simplicity, we consider that particle geodesics do not present backreaction effects. It appears from the results that charged particles can be accelerated to ultrahigh energies in marginally bound orbits near extreme rotating embedded BHs in the presence of magnetic fields. Such a result can help us to understand, for example, high-energy astrophysical phenomena associated with BHs in the universe, in particular, the origin and mechanisms within the acceleration of UHECRs. The sources of UHECRs are still a subject of discussion and BHs are potential particle acceleration sources [46–48].

Suppose that the described BH is surrounded by collisional particles along its possible stable orbits. When considering the motion of particles only under the action of gravity, the conserved quantities along geodesics are the energy and the angular momentum, represented, respectively, by the free-test particle energy in terms of the four-momentum $\bar{p}^\mu$ as

$$\mathcal{E} = -g_{t\mu}\bar{p}^\mu, \tag{30}$$

and the free-test particle angular momentum per unit rest mass

$$\ell = -g_{\phi\mu}\bar{p}^\mu. \tag{31}$$

Such conserved quantities are respectively associated to Killing vectors $\xi_{(t)} = \xi^\mu_{(t)}\partial_\mu = \frac{\partial}{\partial t}$ and $\xi_{(\phi)} = \xi^\mu_{(\phi)}\partial_\mu = \frac{\partial}{\partial \phi}$. Assuming the properties and symmetries presented here are similar to those of a Kerr or a Kerr–Newman BH, we can envisage that when particles are crossing the ergosphere, they acquire negative energy as ascertained by an observer at infinity [49]. In this framework, the scattering process of colliding particles near the horizon of an extremal BH ($a \to 1$) can extract mass and angular momentum from the hole, reaching arbitrarily high center-of-mass energy, i.e., a particular case of the so-called Bañados–Silk–West (BSW) effect [50]. Particle geodesics determined by an effective potential enables the

determination of energy and angular momentum values in which the particles may escape to infinity [51,52]. Additionally, when magnetic fields are present and when a charged particle orbits the ISCO of the embedded BH of Equation (16), an incoming particle can collide, leading to the expelling of the charged particle to infinity, even if $a \leq 0.998$ [47], where $a = 0.998$ is the rotational astrophysical limit, a.k.a. the Thorne Limit [53]. In this case, the presence of magnetic fields may change the frame-dragging aspects of the space-time near the ISCO, permitting the BSW effect for arbitrary values of a.

Consider now two particles, each one with mass m_0, one of them at the ISCO and the other coming from infinity, with energies $\mathcal{E}_1$ and $\mathcal{E}_2$ and different angular momenta ℓ_1 and ℓ_2. In this case, the center-of-mass energy (normalized by the particle mass m_0) of the two-particle system is given by [50]

$$E_{cm} = \sqrt{2}\sqrt{1 - g_{\mu\nu}u^{\mu}_{(1)}u^{\nu}_{(2)}}, \tag{32}$$

where $u^{\mu}_{(1)}$ and $u^{\nu}_{(2)}$ are the four velocities ($u^{\alpha} = \dot{x}^{\alpha} \equiv dx^{\alpha}/d\tau$, where τ is the proper time) of each particle. The four-momentum of the particle reads $\bar{p}_{\mu} = u_{\mu} + qA_{\mu}$, where A_{μ} is the electromagnetic four-potential and q is the charge of the particle. From the Lorentz gauge $A^{\mu}_{;\mu} = 0$, the only nonzero component of the four-potential is $A_{\phi} = Bg_{\phi\phi}/2$, where B is the uniform magnetic field present in the system. Therefore, the conserved quantities in Equations (30) and (31) are written, normalized by the particle mass m_0, as

$$\mathcal{E} = -g_{t\mu}(u^{\mu} + qA^{\mu}), \tag{33}$$

$$\ell = -g_{\phi\mu}(u^{\mu} + qA^{\mu}). \tag{34}$$

Considering the conserved quantities in (33) and (34) ($\mathcal{E}_{(i)} = 1$) and the normalization condition $g_{\mu\nu}u^{\mu}u^{\nu} = -1$, we have the following system of equations:

$$\dot{\phi}_{(i)} = \frac{g_{tt}\ell_i + g_{\phi t}\mathcal{E}_i - g_{tt}g_{\phi\phi}\mathcal{B}}{g_{tt}g_{\phi\phi} - (g_{t\phi})^2}, \tag{35}$$

$$\dot{t}_{(i)} = \frac{-\mathcal{E}_i - g_{t\phi}\dot{\phi}}{g_{tt}}, \tag{36}$$

$$\dot{r}_{(i)} = \sqrt{\frac{-1 - g_{tt}(\dot{t}_{(i)})^2 - 2g_{t\phi}\dot{t}_{(i)}\dot{\phi}_{(i)} - g_{\phi\phi}(\dot{\phi}_{(i)})^2}{g_{rr}}}, \tag{37}$$

where $\mathcal{B} \equiv \frac{qB}{2m_0}$ is the normalized magnetic field strength. Here, we considered for simplicity only equatorial motions (i.e., $\dot{\theta}_{(i)} = 0$).

The center-of-mass collision energy of two particles is calculated from Equation (32). Figures 3 and 4 show the results of the E_{cm} for a set of possible particle angular momenta for BH spins of order $a \sim 0.9$ and BH spins in a near-extremal ($a = 0.99$) regime. Here, we use the permitted range $-2(1 + \sqrt{1+a}) < \ell < 2(1 + \sqrt{1-a})$ [50] for the particle angular momenta. The results presented point to the possibility of particles being expelled to infinity at positions slightly shifted from the BH ISCO which depends on the intensity of B and also on the intensity of α_0. For a fixed value of spin, say $a = 0.9$, larger "extrinsic charge" values α_0 cause accelerations to infinity, even at points relatively far from the event horizon. When the magnetic field is turned on, this effect becomes even more effective. The higher the values of α_0, the greater the chances that the particles will be expelled at positions far from the ISCO. For instance, when $a > 0.9$, the ISCO is located at $1 < r < 1.5$. For the extreme value of $\alpha_0 = 10$, in the presence of magnetic fields, the particle is expelled at $r \sim 5$, far from the ISCO.

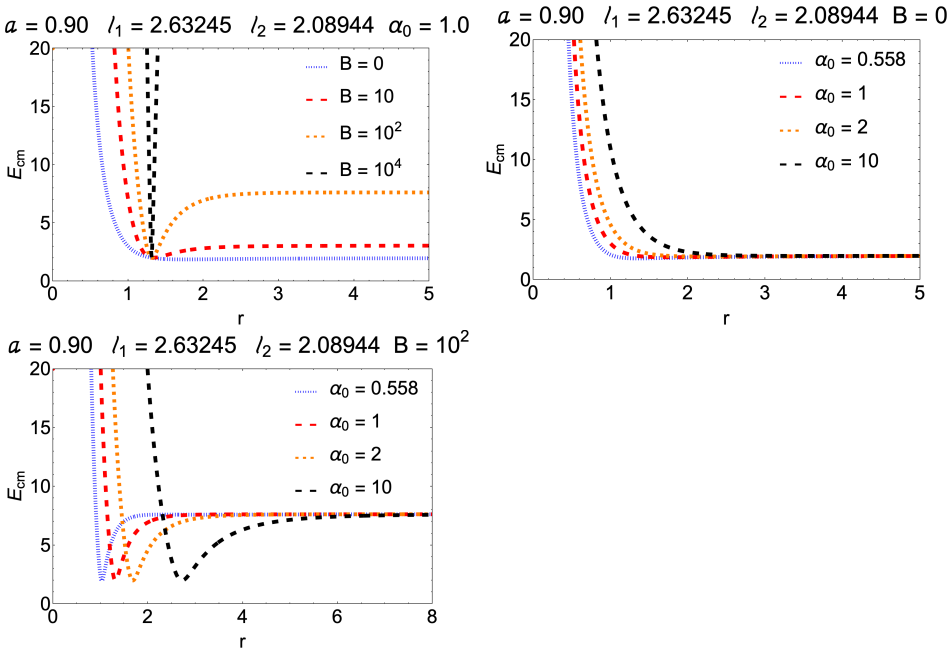

Figure 3. E_{cm} values for $a = 0.9$ and different normalized magnetic field strengths (in C.T/m units).

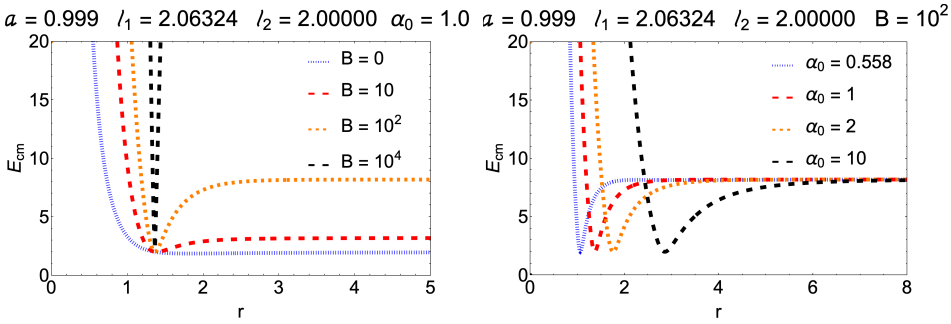

Figure 4. E_{cm} values for $a = 0.999$ and different normalized magnetic field strengths (in C.T/m units).

5. Remarks

By means of the model based on the Nash–Greene theorem, we analyze a Gürses–Gürsey metric embedded in five dimensions. The novelty of this approach is examining the influence of the extrinsic geometry on a rotating "charged" BH. Such characteristics allow us to study this rotating BH as, e.g., a source of UHECRs. In this case, in the presence of a magnetic field, particle acceleration is more efficient. This phenomenon occurs in a nonlinear manner due to the complex relation between the magnetic field and the black hole particle system properties. The effects on the particle acceleration of evolving event horizons and magnetic field dynamics in time-dependent embedded space-times demand future meticulous investigations. Nevertheless, the present picture is a first hint towards the possibility of embedded BHs as efficient accelerators. In particular, specific signatures in the spectrum may even contribute to the understanding of the energy signature proposed here when embedding is introduced into the model. An example of a way to detect such signatures comes from synchrotron radiation. When accelerated particles at the edge of embedded space-time BHs interact with magnetic fields, they deflect and emit synchrotron radiation, which manifests itself in this case as high-energy gamma rays. Thus, the design of experiments in the context of the next large gamma-ray telescopes is essential to understand the signatures arising from phenomena such as those described in this work (see, e.g., [54–58]). Other subjects should also be added to the present study to express a complete picture of a UHECR regarding the many energy features produced by accretion dynamics surrounding the embedded BHs. Furthermore, as expected, there is an increase

in the strength of the gravitational field due to the addition of the extrinsic curvature, and higher values of the extrinsic term lead to an enlargement of the photon ring and an increase in the BH's inner shadow. In terms of prospects, a classical thermodynamic analysis and quasinormal frequencies using the WKB approximation are currently in progress and will be reported elsewhere.

Author Contributions: Conceptualization, A.J.S.C.; formal analysis, C.H.C.-A. and R.d.C.d.A.; methodology, A.J.S.C., C.H.C.-A. and R.d.C.d.A.; software, A.J.S.C. and R.d.C.d.A.; supervision, A.J.S.C.; writing—original draft, A.J.S.C.; writing—review and editing, A.J.S.C., C.H.C.-A. and R.d.C.d.A. All authors have read and agreed to the published version of the manuscript.

Funding: A.J.S.C. acknowledges Conselho Nacional de Desenvolvimento Científico e Tecnologico (CNPq) for the partial financial support for this work (Grant No. 305881/2022-1) and Fundação da Universidade Federal do Paraná (FUNPAR) through public notice 04/2023-Pesquisa/PRPPG/UFPR for the partial financial support (Process No. 23075.019406/2023-92). C.H.C.A. and R.d.C.d.A. gratefully acknowledge the financial support of the "Fenômenos Extremos do Universo" of the Fundação Araucária. The research of R.d.C.d.A. is supported by Conselho Nacional de Desenvolvimento Científico e Tecnológico (CNPq) (310448/2021-2) and (400045/2023-0), Fundação Araucária (698/2022) e (721/2022) and FAPESP (2021/01089-1). She also offers thanks for the support of L'Oreal Brazil, with the partnership of ABC and UNESCO in Brazil.

Data Availability Statement: All data/codes used in this work are publicly available and properly cited in the references.

Conflicts of Interest: The authors declare no conflicts of interest.

References

1. Abbott, B.P.; Abbott, R.; Abbott, T.D.; Abernathy, M.R.; Acernese, F.; Ackley, K.; Adams, C.; Adams, T.; Addesso, P.; Adhikari, R.X.; et al. Observation of Gravitational Waves from a Binary Black Hole Merger. *Phys. Rev. Lett.* **2016**, *116*, 061102. [CrossRef]
2. Arkani–Hamed, N.; Dimopoulos, S.; Dvali, G. The hierarchy problem and new dimensions at a millimeter. *Phys. Lett. B* **1998**, *429*, 263–272. [CrossRef]
3. Israel, W. Singular hypersurfaces and thin shells in general relativity. *Il Nuovo Cimento B (1965–1970)* **1966**, *44*, 1–14. [CrossRef]
4. Randall, L.; Sundrum, R. Large Mass Hierarchy from a Small Extra Dimension. *Phys. Rev. Lett.* **1999**, *83*, 3370–3373. [CrossRef]
5. Randall, L.; Sundrum, R. An Alternative to Compactification. *Phys. Rev. Lett.* **1999**, *83*, 4690–4693. [CrossRef]
6. Maldacena, J. The Large-N Limit of Superconformal Field Theories and Supergravity. *Int. J. Theor. Phys.* **1999**, *38*, 1113–1133. :1026654312961 [CrossRef]
7. Dvali, G.; Gabadadze, G.; Porrati, M. 4D gravity on a brane in 5D Minkowski space. *Phys. Lett. B* **2000**, *485*, 208–214. [CrossRef]
8. Maia, M.; Monte, E.M. Geometry of brane-worlds. *Phys. Lett. A* **2002**, *297*, 9–19. [CrossRef]
9. Maia, M.D.; Monte, E.M.; Maia, J.M.F.; Alcaniz, J.S. On the geometry of dark energy. *Class. Quantum Gravity* **2005**, *22*, 1623. [CrossRef]
10. Maia, M.D.; Silva, N.; Fernandes, M.C.B. Brane-world quantum gravity. *J. High Energy Phys.* **2007**, *2007*, 047. [CrossRef]
11. Nash, J. C1 Isometric Imbeddings. *Ann. Math.* **1954**, *60*, 383–396. [CrossRef]
12. Nash, J. The Imbedding Problem for Riemannian Manifolds. *Ann. Math.* **1956**, *63*, 20–63. [CrossRef]
13. Figueras, P.; Wiseman, T. Gravity and Large Black Holes in Randall-Sundrum II Braneworlds. *Phys. Rev. Lett.* **2011**, *107*, 081101. [CrossRef]
14. Emparan, R. Black Holes in Higher Dimensions. *Living Rev. Relativ.* **2011**, *11*, 6. [CrossRef]
15. Abdolrahimi, S.; Cattoën, C.; Page, D.N.; Yaghoobpour-Tari, S. Spectral methods in general relativity and large Randall-Sundrum II black holes. *J. Cosmol. Astropart. Phys.* **2013**, *2013*, 039. [CrossRef]
16. Abdolrahimi, S.; Cattoën, C.; Page, D.N.; Yaghoobpour-Tari, S. Large Randall–Sundrum II black holes. *Phys. Lett. B* **2013**, *720*, 405–409. [CrossRef]
17. Emparan, R.; Horowitz, G.T.; Myers, R.C. Exact description of black holes on branes. *J. High Energy Phys.* **2000**, *2000*, 007. [CrossRef]
18. Emparan, R.; Horowitz, G.T.; Myers, R.C. Exact description of black holes on branes II: Comparison with BTZ black holes and black strings. *J. High Energy Phys.* **2000**, *2000*, 021. [CrossRef]
19. Meiers, M.; Bovard, L.; Mann, R.B. Charged Randall–Sundrum black holes in higher dimensions. *Class. Quantum Gravity* **2017**, *35*, 025006. [CrossRef]
20. Capistrano, A.J. Constraints on a spherically symmetric 5-d braneworld. *Gen. Relativ. Gravit.* **2013**, *45*, 2647–2660. [CrossRef]
21. Capistrano, A.J.; Gutiérrez-Piñeres, A.C.; Ulhoa, S.C.; Amorim, R.G. On classical thermal stability of black holes with a dynamical extrinsic curvature. *Ann. Phys.* **2017**, *380*, 106–120. [CrossRef]

22. Ulhoa, S.C.; Amorim, R.G.G.; Capistrano, A.J.S. On Quasinormal Modes for Scalar Perturbations of Static Spherically Symmetric Black Holes in Nash Embedding Framework. *Adv. High Energy Phys.* **2017**, *45*, 9891231. [CrossRef]
23. Capistrano, A.J.S. Lukewarm black holes in the Nash-Greene framework. *Phys. Rev. D* **2019**, *100*, 064049. [CrossRef]
24. Schnittman, J.D. The collisional Penrose process. *Gen. Relativ. Gravit.* **2018**, *50*, 77. [CrossRef] [PubMed]
25. Liberati, S.; Pfeifer, C.; Relancio, J. Exploring black holes as particle accelerators: Hoop-radius, target particles and escaping conditions. *J. Cosmol. Astropart. Phys.* **2022**, *2022*, 023. [CrossRef]
26. Tursunov, A.; Stuchlík, Z.; Kološ, M.; Dadhich, N.; Ahmedov, B. Supermassive Black Holes as Possible Sources of Ultrahigh-energy Cosmic Rays. *Astrophys. J.* **2020**, *895*, 14. [CrossRef]
27. Rieger, F.M. Active Galactic Nuclei as Potential Sources of Ultra-High Energy Cosmic Rays. *Universe* **2022**, *8*, 607. [CrossRef]
28. Zajaček, M.; Tursunov, A.; Eckart, A.; Britzen, S. On the charge of the Galactic centre black hole. *Mon. Not. R. Astron. Soc.* **2018**, *480*, 4408–4423. [CrossRef]
29. Zajaček, M.; Tursunov, A. Electric charge of black holes: Is it really always negligible? *arXiv* **2019**, arXiv:1904.04654.
30. Zhuang, M.Y.; Ho, L.C. The Interplay between Star Formation and Black Hole Accretion in Nearby Active Galaxies. *Astrophys. J.* **2020**, *896*, 108. [CrossRef]
31. Juneau, S.; Goulding, A.D.; Banfield, J.; Bianchi, S.; Duc, P.A.; Ho, I.T.; Dopita, M.A.; Scharwächter, J.; Bauer, F.E.; Groves, B.; et al. The Black Hole–Galaxy Connection: Interplay between Feedback, Obscuration, and Host Galaxy Substructure. *Astrophys. J.* **2022**, *925*, 203. [CrossRef]
32. Kotera, K.; Silk, J. ULTRAHIGH-ENERGY COSMIC RAYS AND BLACK HOLE MERGERS. *Astrophys. J. Lett.* **2016**, *823*, L29. [CrossRef]
33. Nagano, M.; Watson, A.A. Observations and implications of the ultrahigh-energy cosmic rays. *Rev. Mod. Phys.* **2000**, *72*, 689–732. [CrossRef]
34. Anchordoqui, L.A. Ultra-high-energy cosmic rays. *Phys. Rep.* **2019**, *801*, 1–93. [CrossRef]
35. Mészáros, P.; Fox, D.B.; Hanna, C.; Murase, K. Multi-messenger astrophysics. *Nat. Rev. Phys.* **2019**, *1*, 585–599. [CrossRef]
36. Spera, M.; Trani, A.A.; Mencagli, M. Compact Binary Coalescences: Astrophysical Processes and Lessons Learned. *Galaxies* **2022**, *10*, 76. [CrossRef]
37. Bejger, M.; Piran, T.; Abramowicz, M.; Håkanson, F. Collisional Penrose Process near the Horizon of Extreme Kerr Black Holes. *Phys. Rev. Lett.* **2012**, *109*, 121101. [CrossRef]
38. Fraschetti, F. On the acceleration of ultra-high-energy cosmic rays. *Phil. Trans. R. Soc. A* **2008**, *366*, 4417–4428. [CrossRef]
39. Gürses, M.; Gürsey, F. Lorentz covariant treatment of the Kerr–Schild geometry. *J. Math. Phys.* **1975**, *16*, 2385–2390. [CrossRef]
40. Greene, R.E. *Isometric Embeddings of Riemannian and Pseudo-Riemannian Manifolds*; Memoirs of the American Mathematical Society: Providence, RI, USA, 1970; 63p. [CrossRef]
41. Maia, M.D.; Capistrano, A.J.S.; Alcaniz, J.S.; Monte, E.M. The Deformable Universe. *Gen. Rel. Grav.* **2011**, *43*, 2685–2700. [CrossRef]
42. Capistrano, A.J.S.; Cabral, L.A.; Marão, J.A.P.F.; Coimbra-Araújo, C.H. Linear Nash-Greene fluctuations on the evolution of S8 and H0 tensions. *Eur. Phys. J. C* **2022**, *82*, 1434–6052. [CrossRef]
43. The Sage Developers. *SageMath, the Sage Mathematics Software System (Version 10.2)*; 2023. Available online: https://www.sagemath.org (accessed on 23 August 2024).
44. Capistrano, A.a.J.S.; Nunes, R.C.; Cabral, L.A. Lower tensor-to-scalar ratio as possible signature of modified gravity. *Phys. Rev. D* **2024**, *109*, 123517. [CrossRef]
45. Aghanim, N.; et al. Planck 2018 results—VI. Cosmological parameters. *Astron. Astrophys.* **2020**, *641*, A6. [CrossRef]
46. Harada, T.; Kimura, M. Black holes as particle accelerators: A brief review. *Class. Quantum Gravity* **2014**, *31*, 243001. [CrossRef]
47. Pereira, J.P.; Coimbra-Araújo, C.H.; dos Anjos, R.C.; Coelho, J.G. Binary Coalescences as Sources of Ultrahigh-Energy Cosmic Rays. *Phys. Rev. Lett.* **2024**, *132*, 091401. [CrossRef]
48. Anjos, R.C.; Coimbra-Araújo, C.H. Central accumulation of magnetic flux in massive Seyfert galaxies as a possible engine to trigger ultrahigh energy cosmic rays. *Phys. Rev. D* **2017**, *96*, 023008. [CrossRef]
49. Bardeen, J.M.; Press, W.H.; Teukolsky, S.A. Rotating Black Holes: Locally Nonrotating Frames, Energy Extraction, and Scalar Synchrotron Radiation. *Astrophys. J.* **1972**, *178*, 347–370. [CrossRef]
50. Bañados, M.; Silk, J.; West, S.M. Kerr Black Holes as Particle Accelerators to Arbitrarily High Energy. *Phys.Rev.Lett.* **2009**, *103*, 111102. [CrossRef]
51. Coimbra-Araújo, C.H.; dos Anjos, R.C. Acceleration of charged particles from near-extremal rotating black holes embedded in magnetic fields. *Class. Quantum Gravity* **2021**, *38*, 015007. [CrossRef]
52. Coimbra-Araújo, C.H.; dos Anjos, R.C. Ultra-High-Energy Particles at the Border of Kerr Black Holes Triggered by Magnetocentrifugal Winds. *Galaxies* **2022**, *10*, 84. [CrossRef]
53. Thorne, K.S. Disk-accretion onto a black hole. II. Evolution of the hole. *Astrophys. J.* **1974**, *191*, 507–520. [CrossRef]
54. Murase, K. High-energy emission induced by ultra-high-energy photons as a probe of ultra-high-energy cosmic-ray accelerators embedded in the cosmic web. *Astrophys. J. Lett.* **2012**, *745*, L16. [CrossRef]
55. Inoue, S.; Granot, J.; O'Brien, P.T.; Asano, K.; Bouvier, A.; Carosi, A.; Connaughton, V.; Garczarczyk, M.; Gilmore, R.; Hinton, J.; et al. Gamma-ray burst science in the era of the Cherenkov Telescope Array. *Astropart. Phys.* **2013**, *43*, 252–275. [CrossRef]
56. Berezinsky, V.; Gazizov, A.; Kalashev, O. Cascade photons as test of protons in UHECR. *Astropart. Phys.* **2016**, *84*, 52–61. [CrossRef]

57. The CTA Consortium. *Science with the Cherenkov Telescope Array*; World Scientific: Hackensack, NJ, USA, 2019. [CrossRef]
58. Zhen, C.; Ming-jun, C.; Song-zhan, C.; Hong-bo, H.; Cheng, L.; Ye, L.; Ling-ling, M.; Xin-hua, M.; Xiang-dong, S.; Han-rong, W.; et al. Introduction to Large High Altitude Air Shower Observatory (LHAASO). *Chin. Astron. Astrophys.* **2019**, *43*, 457–478. [CrossRef]